Self-powered communicating wireless sensor with flexible aero-piezoelectric energy harvester

Julien Le Scornec, Benoit Guiffard, Raynald Seveno, Vincent Le Cam, Stephane Ginestar

Self-powered communicating wireless sensor with aero-piezoelectric energy harvester

Julien Le Scornec[1]*, Benoit Guiffard[2], Raynald Seveno[2], Vincent Le Cam[1] and Stephane Ginestar[2]

[1] Université Gustave Eiffel, COSYS/SII, Route de Bouaye, 44344 Bouguenais, France

[2] IETR UMR CNRS 6164, UBL University, University of Nantes, 2 rue de la Houssinière, 44322 Nantes Cedex 3, France

E-mail: julien.le-scornec@univ-eiffel.fr

Abstract

This paper presents an ultra-flexible piezoelectric air flow energy harvester capable of powering a wireless sensor. The method to easily adapt the aero-electric generator to the wind is presented. In the wind tunnel, different configurations have been tested to determine the best one for energy harvesting at low wind speed. In particular, the galloping configuration, with the addition of a bluff body at the free end of the cantilever which allows to improve the performance of the micro-generator by coupling the vibrations induced by the vortices and the galloping phenomena. In this study, we also present a method to optimize the energy harvesting without increasing the volume of the device. The effects of mechanical and electrical coupling of several generators on the performance of energy harvesting are presented. Thus, with the electrical parallel coupling of four generators, we obtained a maximum power of 60 mW instead of 30 mW with two generators for a wind speed of about 6 m/s. The mechanical coupling of the micro-generators allowed the device to keep the same volume (z540 cm3), however the threshold wind speed to increase (>6 m/s). The harvested energy was then used to operate a wireless sensor.

Keywords: Aero-electric energy harvester; piezoelectric micro-generator; cantilever configuration ultra-flexible; wireless sensor

1 INTRODUCTION

Nowadays, wireless communicating sensors are an integral part of our daily lives, present in industry, transportation, building health, military and space. They are most often scalable and are distributed alone or in a network. They allow the user to physically adapt the instrumentation deployed in the field to the application. For this reason, wireless systems are increasingly demanding energy performance. Micro energy harvesting has many advantages for powering wireless sensors in terms of increased lifetime, reduced maintenance efforts and economic cost. The other advantage is to limit the environmental impact of sensors by limiting the use of batteries that are too polluting. Recent technological developments have allowed the extraction of renewable energy from various sources such as the sun, geothermal energy, wind, vibrations. Naturally, wind energy is of strong interest for its unique properties, such as renewable energy, ubiquitous, freely available and environmentally friendly [1,2]. However, the efficiency of the wind energy to electricity conversion system based on remains low. Many researches have been conducted to improve the efficiency of wind energy conversion into electrical energy. To convert this mechanical energy into electrical energy, different transduction mechanisms exist, we can cite electromagnetic [3,4], electrostatic [5], triboelectric [6,7] and piezoelectric [8–10] mechanisms. By their nature, piezoelectric materials are one of the most used means because of their high power density and ease of implementation. Regarding the source of vibration, research can be classified into structural, acoustic, thermoacoustic and aero-elastic energy harvesting vibrations. For example, random excitations [11], flow-induced vibrations [12] or other nonlinear vibrations [13] might be mentioned. Aero-electric energy harvesting exploits the vibrations of elastic structures in an airflow. It is based on the generation of aero-elastic vibrations, which can be obtained from the well-known phenomena of vibration induced by vortex and galloping.

In the field of piezoelectric thin films, several materials such as $Pb(Zr,Ti)O_3$ (PZT), ZnO, and AlN have been widely studied [14–16]. However, due to its outstanding ferroelectric and piezoelectric properties, PZT is the most attractive candidate for energy harvesting. In our laboratory, piezoelectric thin films were prepared by a chemical deposition process on a commercial aluminum (Al) substrate [17] (low cost and easily transferable in industry). An electrode is deposited on the surface of the PZT to obtain a micro-generator with a Metal Insulating Metal (MIM) electrodes structure. To increase the energy efficiency of the generator, we used the interdigitated electrodes structure (IDE). This structure allows to reduce the linear capacitance of the generator and thus increase the harvested power [18]. To design the IDE structure, the PZT films must be separated from the aluminum foil and transferred onto an insulating polymer in order to remove the ground plane. The solution used by Park et al [19] is to deposit a PZT thin film on a sapphire for the crystallization step. Then, using a laser lift-off (LLO) process, they transferred the film onto a polymer sheet. However, this method may be difficult to transfer to industry for mass production. Another technique [20] consists in depositing PZT on an aluminum foil and transferring this layer to a flexible and insulating polymer. Then, the aluminum foil is chemically etched before finally depositing electrodes on the PZT surface. In this way, the lightness of the micro-generator is preserved and makes it sensitive to air flow.

The above studies have made significant progress in the development of piezoelectric wind energy harvesting. However, improving the efficiency of the piezoelectric micro-generator under air flow is still a priority for researchers. In this paper, we present the procedure for obtaining a cantilever-based ultra-flexible micro-generator for wind energy harvesting. The procedure allows the thickness of the beam-shaped micro-generator to be easily adapted to wind source for an energy harvesting application. Thus, changing the thickness directly influences the neutral line, which in turn impacts the energy performance of the generator. The power output and performance of the micro-generator under airflow is improved by adding an obstacle in front of the cantilever or a bluff body attached at the free end of the beam. Comparisons in wind tunnel are conducted between the piezoelectric micro-generator in horizontal, horizontal with obstacle and galloping configurations in terms of output voltages. In this paper, we highlight the mechanical and electrical coupling of an assembly of several generators in order to increase the output energy density without increasing the system footprint. The coupling of the

generators allowed powering a wireless communicating temperature sensor during several measurements and temperature transitions.

The article is organized as follows. In the first section, the background of this study is introduced, followed by the second section, which describes the design of a micro-generator. The third section reviews the results obtained based on the different configurations (horizontal, horizontal with obstacle and galloping) used in the wind tunnel and the coupling of several generators and conclusions are drawn in the last section.

2 FABRICATION PROCESS AND EXPERIMENT SETUP

2.1 Fabrication process

The fabrication techniques mainly involve the preparation of PZT thin films on commercial aluminum foils, the photolithography step, and the transfer onto polymers. Most of the process steps were performed in a standard clean room environment. The basic fabrication process of PZT micro-generators is detailed in previous paper [18].

The fabrication process begins with the deposition of a PZT thin film on a commercial aluminum foil by a chemical solution deposition (CSD) process. The precursor solution is prepared by mixing lead acetate trihydrate [$Pb(CH_3CO_2)_2$, $2H_2O$], zirconium [$Zr(O(CH_2)_2CH_3)_4$] and titanate [$Ti((CH_3)_2CHO)_4$] n-propoxides to obtain the optimal composition [21,22], namely $Pb_{1.3}(Zr_{0.57},Ti_{0.43})O_3$. To reduce the appearance of cracks during the heat treatment of the films, ethylene glycol [$HO\text{-}CH_2\text{-}CH_2OH$] is added to the solution. The resulting solution is deposited on the aluminum foil at 6000 rpm for 20 s by a spin coating process and then annealed for 2 min in an open air oven preheated to 650° C. Each layer has a thickness of 300 nm, to obtain a 3 µm-thick PZT film, the deposition and annealing steps are repeated 9 times.

On the surface of the PZT, we designed an interdigitated electrodes structure (IDE) by "lift-off" photolithography. This electrodes structure consists of two interdigitated combs, 20 gold fingers of 1.3 cm length, 200 µm width and 100 µm space between two fingers. A polymer resin is then deposited on the surface by spin coating process, it allows to create an adhesion layer for the polymer film. The PZT film with the IDE structure is then thermally bonded to a polymer film (Polyethylene Terephthalate, PET) in order to remove the ground plane (aluminum substrate) by chemical etching [23,24]. Finally, the active material is completely encapsulated in the PET. This process allows to obtain a flexible micro-generator at low cost and possibly transferable in the industry. The polarization of the piezoelectric film on a hot plate at 100° C is achieved with a continuous electric field of 100 kV/cm applied for about 2 hours.

The process used in this study to design the micro-generators allows controlling the thickness of the polymer layer that encapsulates the active material. This also allows controlling the position of the neutral line and the flexibility of the micro-generator. For a piezoelectric micro-generator that converts mechanical energy of deformations into electrical energy, the neutral line plays a very important role. When a cantilever beam is subjected to forces that tend to bend it, the upper fibers compress and the lower fibers stretch, while the neutral axis does not change in length. The compression or elongation of the fibers is proportional to their distance from the neutral axis.

The position z_{NA} of the neutral axis [25] (taking the free surface of the supporting PET layer as origin $z = 0$) is given by:

$$z_{NA} = \frac{\sum_{i=1}^{n} \overline{E}_i t_i z_i}{\sum_{i=1}^{n} \overline{E}_i t_i} \quad (1)$$

With *n* the number of layers, $\overline{E}_i = E_i/(1 - v_i)$ is the plane deformation modulus of the *i* -layer (E_i and v_i are respectively the Young's modulus and the Poisson's ratio), t_i the thickness of the *i* -layer and z_i the position of the median plane of the *i*- layer.

Thus, to optimize the piezoelectric micro-generator, we made a compromise between the neutral line that must be the farthest from the active material and the flexibility of the micro-generator, which depends on the thickness of the supporting PET layer.

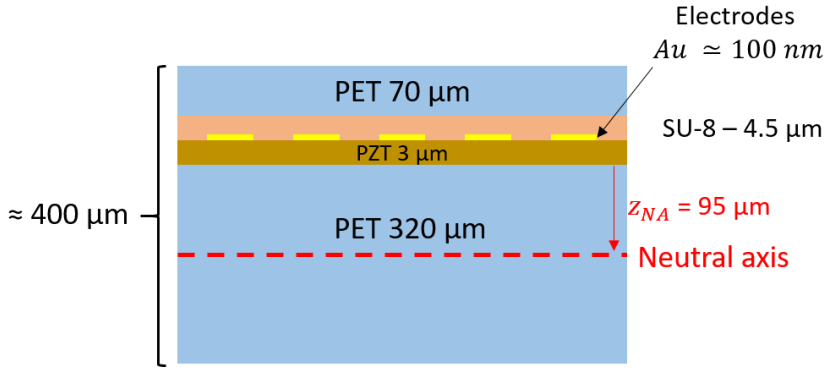

Fig 1 : Scheme of the cross-section of the micro generator.

In order to keep a high flexibility as well as a high energy efficiency, we used a 320 µm PET sheet as supporting substrate (Fig 1). Thus, the neutral line is positioned at 95 µm from the active material (PZT). The encapsulation of the active material in a polymer also allows protecting the micro generator from large deformations. It can thus tolerate a maximum bending radius of 2.2cm (Fig 2 (a)) and important transverse deformations (Fig 2 (b)).

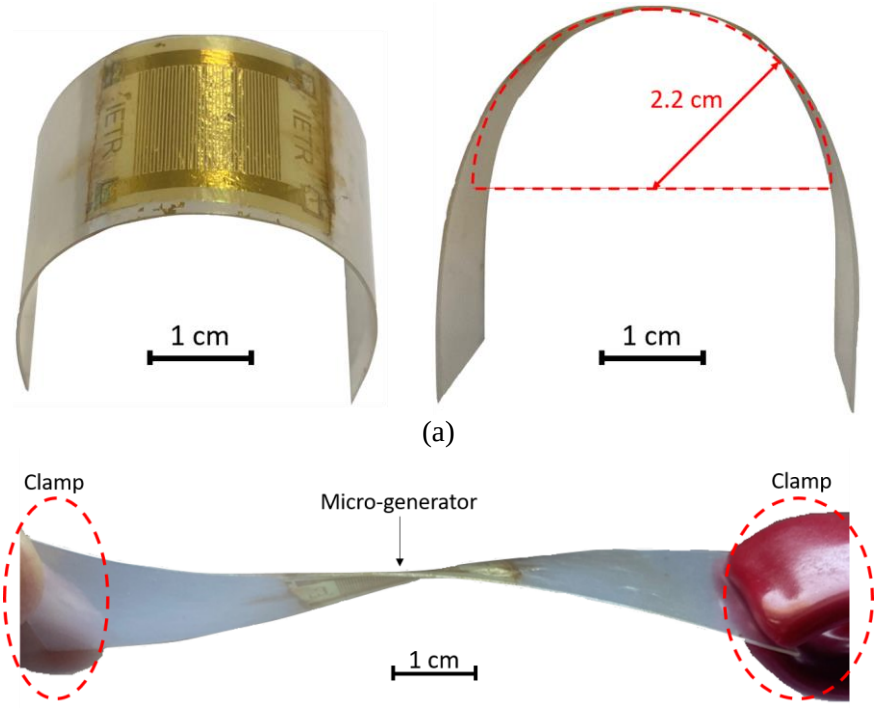

Fig 2 : (a) Deformation of the micro generator with a radius of curvature of 2.2 cm and (b) transverse deformations of the micro generator

2.2 *Experimental setup*

The experimental configuration of the micro-generator in the wind tunnel is given in Fig 3. The wind tunnel is made of plexiglass with a metal honeycomb grille inside to ensure uniformity and stability of the incoming wind. A draft fan regulated by a potentiometer controls the wind speed in the tunnel. Due to the properties of the fan controller, we use an anemometer (Testo 425) with an accuracy of 0.1 m/s to measure the wind speed in the tunnel.

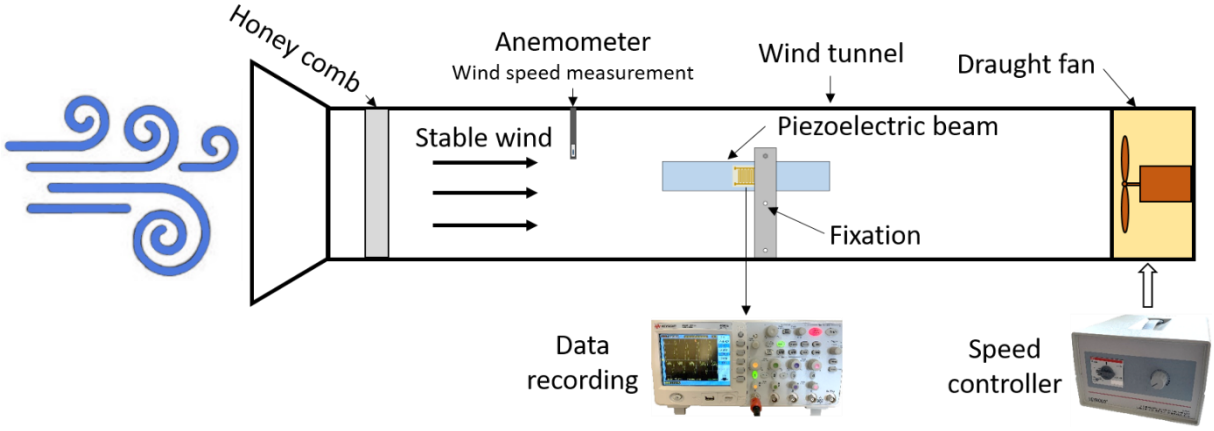

Fig 3 : Schematic of the wind tunnel experiment setup.

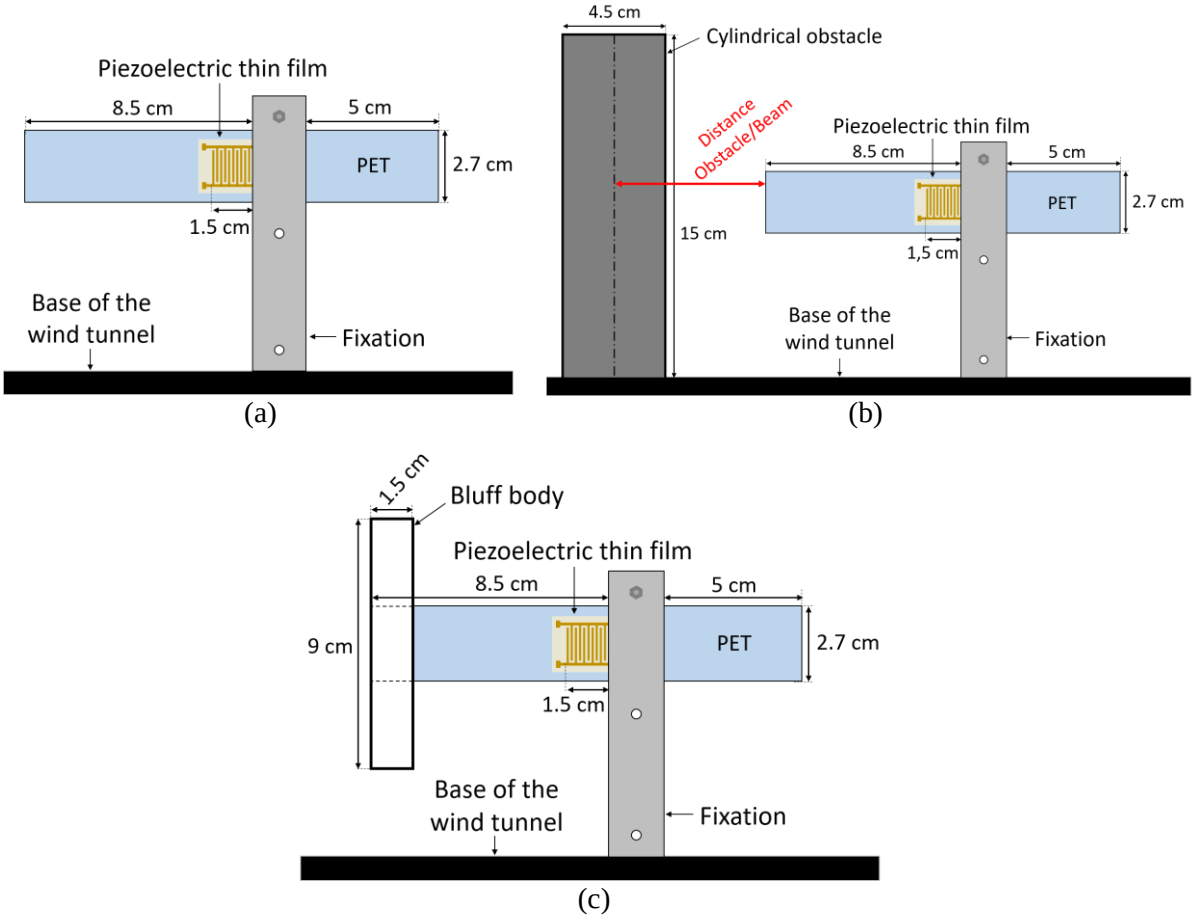

Fig 4 : Schematic of the different configurations carried out in the experiment: (a) horizontal configuration, (b) horizontal configuration with obstacle and (c) galloping configuration.

In this experiment, the cantilever beam and the piezoelectric micro-generator (attached near fixed end of the cantilever beam) are respectively made of Polyethylene Terephthalate (PET) and a PZT thin film (3µm). The energy harvester prototype is firmly clamped by two metal fixings and placed in a wind

tunnel. The dimensions of the cantilever beam are L × W × h_b = 85 × 27 × 0.4 mm^3. On the Fig 4 is shown the three tested configurations, horizontal, horizontal with obstacle and galloping. For the horizontal configuration with obstacle (Fig 4 (b)), a cylindrical obstacle (15 cm high and 4.5 cm in diameter) is placed at 8 cm between the wind and the micro-generator in order to create turbulences at the level of the beam. This allows increasing the deformations of the micro-generator. For the galloping configuration (Fig 4 (c)), the bluff body (polystyrene) (1.5 cm x 1.5 cm x 9 cm) is attached directly at the free end of the beam.

For each configuration tested, the voltage across the micro-generator is recorded using a Tektronix TBS 1052B-EDU oscilloscope for different wind speeds (from 2 to 12 m/s). The frequency and voltage responses were recorded for the distribution of wind speed and load resistances of 1, 5, 10, 50, 100 MΩ with voltage probe and 200 MΩ and 500 MΩ with voltage divider bridge. Thus, for each wind speed, the steady-state voltage signal is recorded, and the root-mean-square (RMS) of the response is calculated. The internal capacitance of the piezoelectric micro-generator is approximately 60 pF.

3 RESULTS AND DISCUSSION

The voltages generated by the micro-generator in horizontal configuration with and without obstacle for a wind speed of about 6 m/s are presented in Fig 5. The voltage measurements were performed across a 100 MΩ load resistor. The generated voltage is very unstable with a very low amplitude around 2 V for the horizontal configuration without obstacle and around 20 V for the horizontal configuration with obstacle. These measurements show that it is possible to recover energy, but that it is difficult to quantify it as the signals are so unstable.

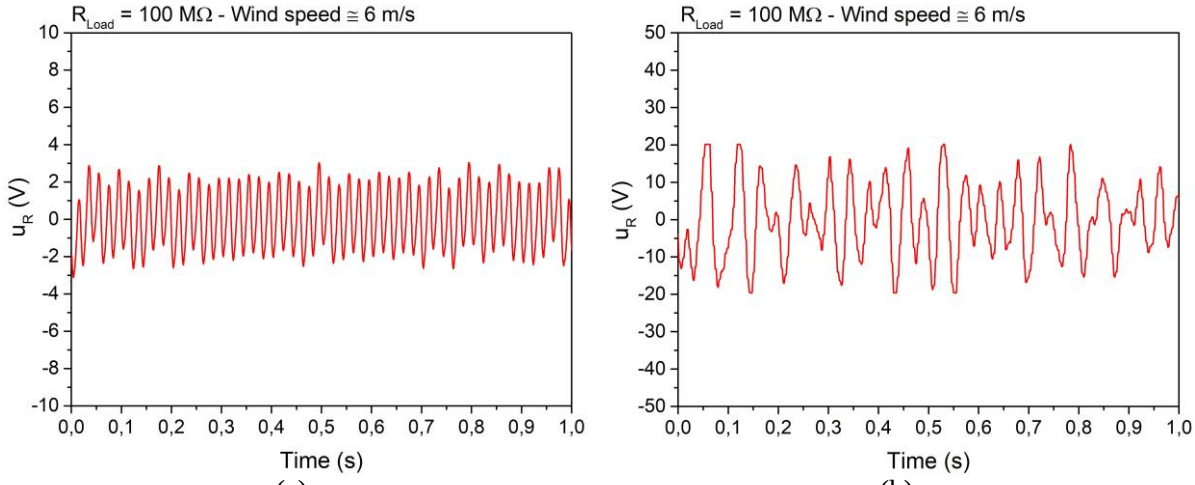

Fig 5 : Voltage delivered by the micro-generator in horizontal configuration a) without obstacle and b) with obstacle for a wind speed of around 6 m/s at 100 MΩ.

The recorded signals show excitations at very different frequencies. The observed vibration frequency for the unobstructed horizontal configuration at 6 m/s (≈ 50 Hz) is much higher than that observed at 10 m/s (≈ 14 Hz). With the horizontal configuration with obstacle, the observed vibration frequency is27 Hz at 6 m/s and it is about 16 Hz at 12 m/s for the horizontal configuration with obstacle.

Fig 6 (a) and Fig 6 (b) present the comparisons in frequency and RMS voltage of the micro-generator for the different studied configurations (horizontal, horizontal with obstacle and galloping) as a function of wind speed. For the horizontal configuration, the energy harvesting is maximized with a wind speed of 9 m/s (Fig 6 (b)). Between 6 and 8 m/s the voltage delivered by the micro-generator is about 2 V, this voltage rises up to 5 V at 9 m/s and remains stable. The addition of the obstacle (horizontal configuration with obstacle) allowed to increase the deformation of the micro-generator and thus to increase the energy harvesting. The voltage was multiplied by 4, going from 5 V with the horizontal configuration without

obstacle to 22 V for the horizontal configuration with obstacle. However, the voltages generated with these two configurations are very unstable and low.

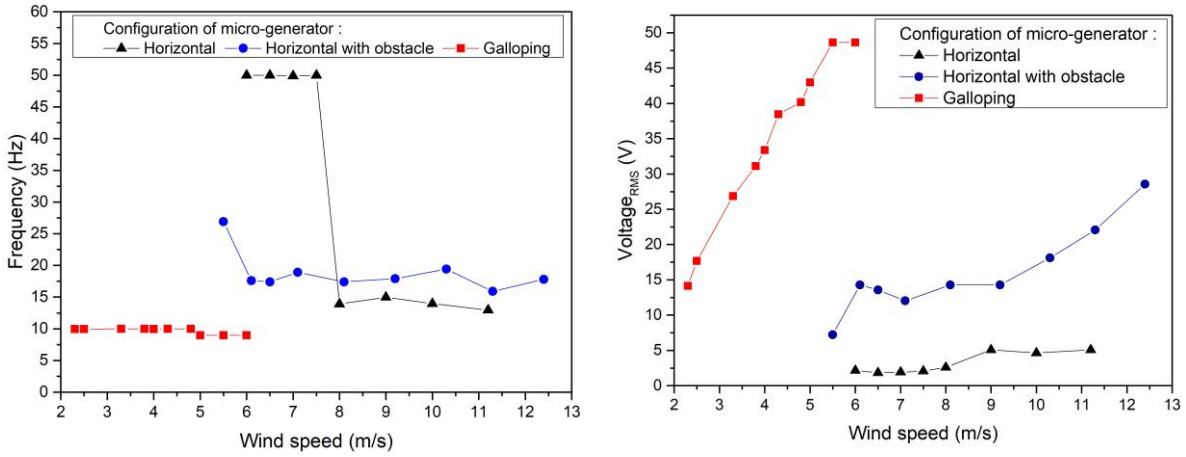

(a) (b)

Fig 6 : Evolution of (a) frequency and (b) RMS voltage delivered by the micro generator across a 100 MΩ load resistor as a function of wind speed for the different studied configurations.

The horizontal configurations without and with obstacle do not allow the micro-generator to have a large amplitude of deformation despite its high flexibility. With these two configurations, the micro-generator requires high wind speeds (> 6 m/s).

The experimental results of the micro-generator in galloping configuration (Fig 4 (c)) for wind speeds of 2.3 m/s and 6 m/s are shown in Fig 7. The voltage measurements were performed across a 100 MΩ load resistor. Fig 7 (a) shows that the micro-generator starts to operate efficiently from a wind speed of 2.3 m/s with a stable voltage and amplitude of 20 V. The amplitude of the voltage generated by the micro-generator increases with the wind speed to reach 70 V at 6 m/s (Fig 7 (b)). This is explained by the fact that the amplitude of the mechanical deformation undergone by the PZT thin film increases with the wind speed.

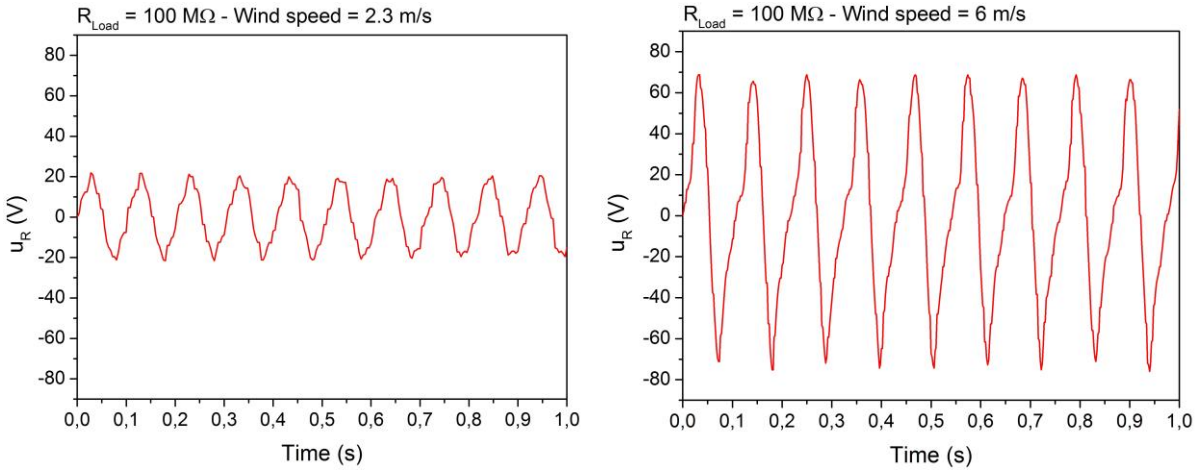

(a) (b)

Fig 7 : Voltage signals delivered by the micro-generator in horizontal configuration for a wind speed of (a) 2.3 m/s and (b) 6 m/s at 100 MΩ.

The observed vibration frequency for the galloping configuration is stable as a function of wind speed (≈ 10 Hz) unlike the other two configurations. Fig 6 (b) shows that the RMS voltage increases with wind speed to reach 50 V peak at 6 m/s, while for the same wind speed, the voltage for the horizontal and horizontal configuration with an obstacle is 2.5 V and 15 V respectively.

The galloping configuration is very simple to implement and it allows the micro-generator to deliver quasi-sinusoidal voltages with higher amplitudes. Contrary to the two other configurations seen previously (Fig 5), the micro-generator can operate efficiently from 2.3 m/s. This study has also

highlighted the mechanical limits of the generator in the wind. Beyond 6 m/s, it undergoes too important deformations which can damage it.

Another characterization was performed by measuring the U_R output voltage amplitude for five different load resistors at a fixed frequency (10 Hz), corresponding to the resonance frequency of the micro-generator in galloping configuration (Fig 6 (a)). This experiment was performed for different wind speeds from 2.3 to 6 m/s.

From these measurements, we can deduce the voltage amplitude U_R, the current amplitude I_R and the generated power P through the load resistance R by using equations (3) and (4), where I_0 is the piezoelectric current, C is the capacitance of one generator and ω is the angular frequency. Theoretical curves were obtained by using equations (2) and (4).

$$I_R = \frac{I_0}{\sqrt{1 + R^2C^2\omega^2}} \tag{2}$$

$$U_R = R \times I_R \tag{3}$$

$$P = \frac{U_R \times I_R}{2} = \frac{{I_0}^2 \times R}{2(1 + (RC\omega)^2)} \tag{4}$$

The theoretical and experimental data of voltage, current and power managed by the micro-generator for different wind speeds are plotted (Fig 8 and Fig 9) with load resistances (1, 5, 10, 50, 100, 200 and 500 MΩ). A good agreement between experiment and theory is observed. Thus, the value of the load resistance giving the maximum power is consistent with the calculated value $R_{opt} = 1/C\omega$ obtained by deriving the power expression [Eq. (4)] as a function of R. The theoretical value of the optimum resistance is $R_{opt} \approx 265$ MΩ at 10 Hz since the sample has a very low capacitance C around 60 pF.

$$P_{max} = \frac{I_0^2}{4C\omega} \tag{5}$$

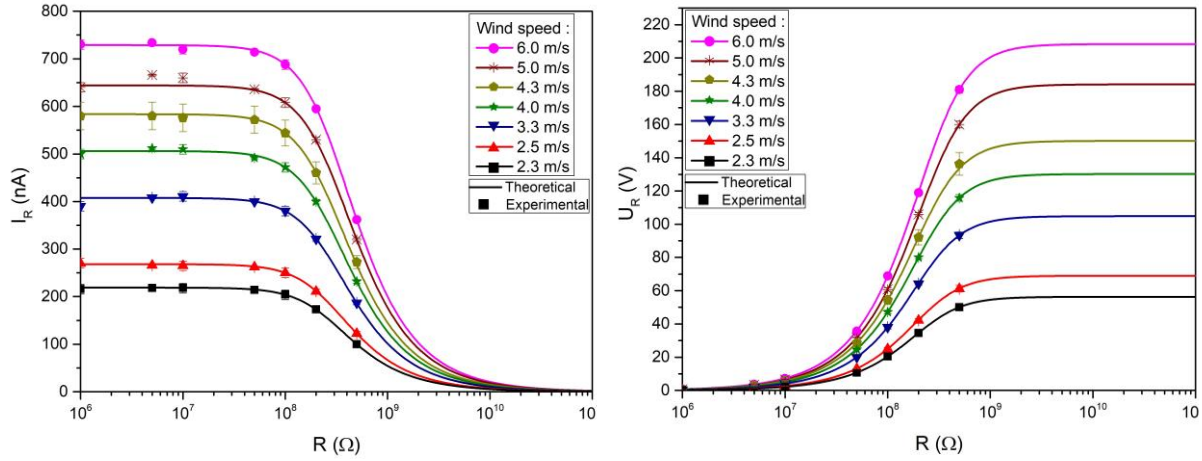

Fig 8 : (a) Current and (b) voltage amplitudes delivered by the micro-generator for different wind speeds according to the load resistance.

Fig 8 (a) highlights the influence of the wind speed on the energy harvesting, with a piezoelectric current I_0 that increases significantly from 215 nA for a wind speed of 2.3 m/s to 730 nA with a wind speed of 6 m/s. The open circuit voltage amplitude delivered by the generator varies according to the wind speed (Fig.8(b)). It reaches about 200 V for a wind speed of 6 m/s, and drops to 40 V with a wind speed of 2.3 m/s.

Similarly, the maximum power (at $R_{opt} = 1/C\omega$) increases with wind speed (Fig 9 (a)). Thus, it increases from 3 µW for a wind speed of 2.3 m/s to 38 µW for a wind speed of 6 m/s. The evolution of the maximum power delivered by the micro-generator as a function of the wind speed is plotted in Fig 9 (b). This figure shows the evolution of the maximum power ($R_{load} = R_{opt}$) harvested as a function of

wind speed. The increase of the maximum power is mainly due to the piezoelectric current which increases with the wind speed due to the higher deformation of the beam. With the galloping configuration, the micro-generator can generate a stable sinusoidal voltage from 2.3 m/s and yields a maximum power of 38 µW at 6 m/s.

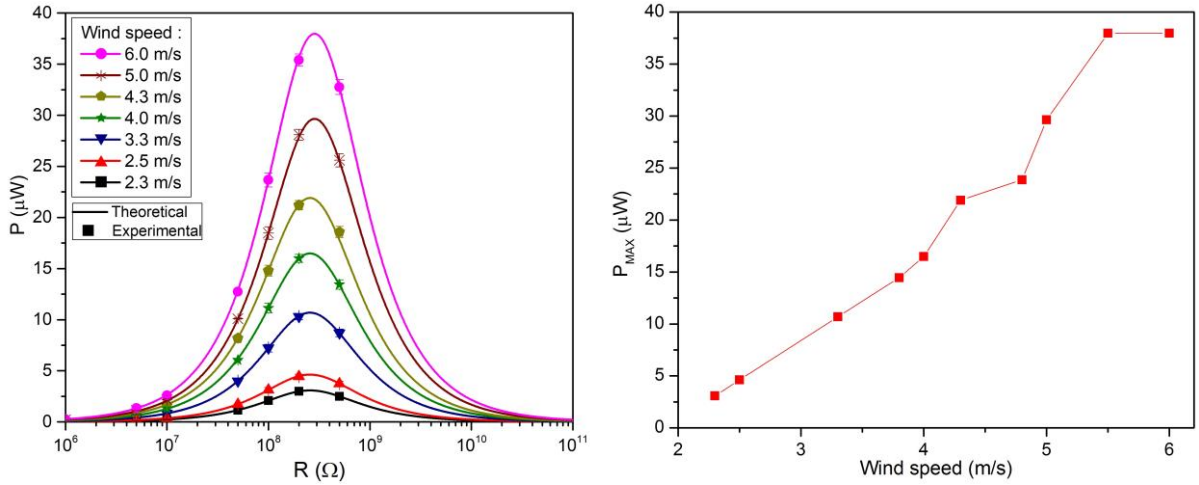

(a) (b)

Fig 9 : (a) Power delivered by the micro-generator for different wind speeds as a function of load resistance and (b) evolution of the maximum power delivered by the micro-generator according to the wind speed.

In the literature, there is a wide range of piezoelectric generators for aeroelectric energy harvesting in a galloping configuration. However, in the literature very few use an interdigitated electrode (IDE) structure for aeroelectric energy harvesting. Table 1 summarizes the main characteristics of flexible piezoelectric micro-generators found in the literature (including polymer/polymer and hybrid oxide/polymer bilayer structure) with a Metal/Insulator/Metal (MIM) electrodes structure and allowing a comparison with the micro-generator developed in the present study. It should be noted that the power density (surface and volume) of the micro-generator depends on the beam shape, active area, thickness and wind speed. Nevertheless, the data collected for wind speeds between 3 m/s and 8 m/s show that the surface power density (21 µW/cm^2) with the generator presented in this work is in the average of those reported in the literature. However, the volume power density (70185 µW/cm^3) of the developed micro-generator is much higher than those reported in the literature. This is due to the thickness of our active material which is much smaller than that of the literature, 3 µm against 180 µm on average.

	Piezoelectric material [substrate]	Electrodes	Thickness of active material	Active area	Wind speed	Power max	Power density surface	Power density volume
Zhang and al. [26]	PVDF [metal]	MIM	28 µm	6.6 cm^2	8.0 m/s	50.2 µW	7.6 µW/cm^2	2714.2 µW/cm^3
He and al. [27]	PVDF [PET]	MIM	200 µm	2.3 cm^2	6.0 m/s	60.9 µW	26.5 µW/cm^2	1325.0 µW/cm^3
Sun and al. [28]	MFC P2 types [aluminum]	MIM	300 µm	3.9 cm^2	6.0 m/s	74.5 µW	19.1 µW/cm^2	636.6 µW/cm^3
Yang and al. [29]	PVDF [PET]	MIM	200 µm	1.6 cm^2	5.0 m/s	69.4 µW	43.4 µW/cm^2	2170.0 µW/cm^3
Sun and al. [30]	PVDF [aluminum]	MIM	28 µm	4.0 cm^2	6.0 m/s	24.8 µW	6.2 µW/cm^2	2214.2 µW/cm^3
Qui and al. [31]	PZT [aluminum]	MIM	150 µm	0.2 cm^2	6.0 m/s	0.5 µW	2.5 µW/cm^2	9.2 µW/cm^3
Wang and al. [32]	MFC P2 types [metal]	MIM	300 µm	2.0 cm^2	6.0 m/s	57.8 µW	28.9 µW/cm^2	963.3 µW/cm^3
Wang and al. [33]	PZT-5 [aluminum]	MIM	120 µm	3.9 cm^2	3.0 m/s	63.2 µW	16.2 µW/cm^2	1350.0 µW/cm^3
Wang and al. [34]	PZT-5 [aluminum]	MIM	120 µm	7.2 cm^2	4.3 m/s	142.6 µW	19.8 µW/cm^2	229.1 µW/cm^3
Zhang and al. [35]	PZT-5 [copper]	MIM	250 µm	4.8 cm^2	6.0 m/s	30.2 µW	6.3 µW/cm^2	252.0 µW/cm^3
Shi and al. [36]	PVDF [PET]	MIM	28 µm	1.5 cm^2	6.0 m/s	4.9 µW	3.3 µW/cm^2	1178.6 µW/cm^3
Zhang and al. [37]	PZT-5 [copper]	MIM	250 µm	6.0 cm^2	8.0 m/s	99.6 µW	16.6 µW/cm^2	664.0 µW/cm^3
Hu and al. [38]	MFC P2 types [aluminum]	MIM	300 µm	3.9 cm^2	3.5 m/s	99.4 µW	25.5 µW/cm^2	850.0 µW/cm^3
This work	PZT[PET]	IDE	3 µm	1.8 cm^2	6.0 m/s	37.9 µW	21.0 µW/cm^2	70185.0 µW/cm^3

Table 1 : Characteristics of flexible piezoelectric generators in galloping configuration.

3.1 *Coupling of micro-generators*

The objective of this work is to harvest energy from air flows, thus a study on the mechanical and electrical coupling of two generators with an IDE structure was carried out. For this purpose, the two generators are glued between each other to form a single beam. Fig 10 shows a schematic of the association of the two generators. The beam has a width of 2.7 cm and a length of 8.5 cm. The association of the two generators induces a shift of the neutral line to the center of the beam (320 µm from the active material) but also an increase the resonance frequency. The previous study on the energy efficiency of a micro-generator under air flow according to different configurations has highlighted the advantages of the galloping configuration for energy harvesting. For the coupled generators, we thus use the galloping configuration with a bluff body (1.5 cm x 1.5 cm x 9 cm) fixed at its free end.

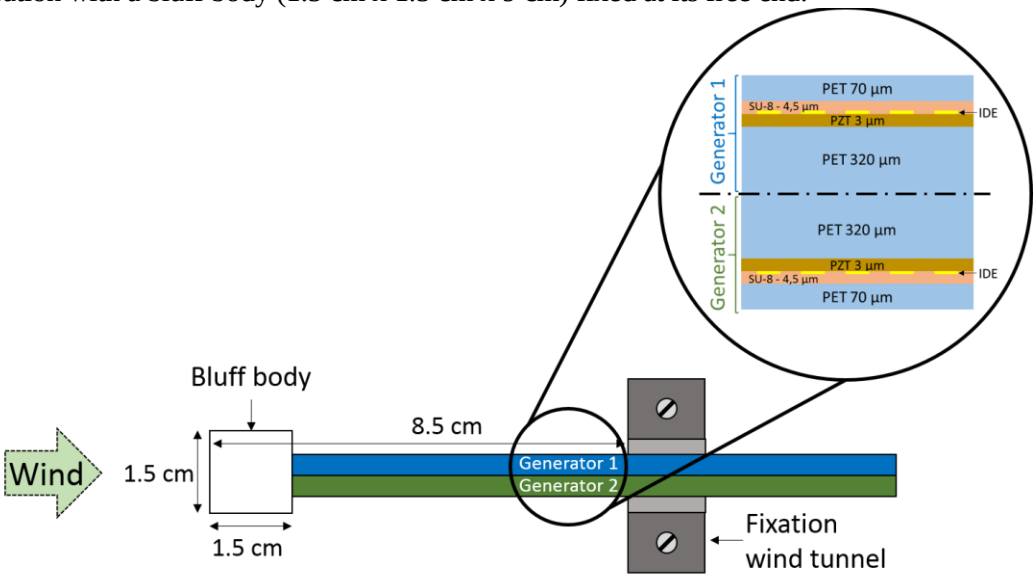

Fig 10 : Representation of the top view of the bi-generator beam in galloping configuration.

The mechanical coupling of the micro-generators allows to double the number of generators without increasing the dimensions of the device. Thus, the two generators will deform simultaneously, which makes them electrically coupled (series or parallel coupling). With electrical coupling, it is important to pay attention to the direction of connection of one micro-generator with respect to the other one. In this configuration (Fig 10), when a force is applied to the beam, generator 1 becomes stretched while generator 2 is compressed (Fig 11 (a)). A positive voltage appears at the terminals of the generator when it stretches and a negative voltage when it compresses. In this study, for the electrical coupling, the generators were connected in reverse of each other so that their respective output voltages are in phase (i.e. they do not cancel each other) (Fig 11 (b)).

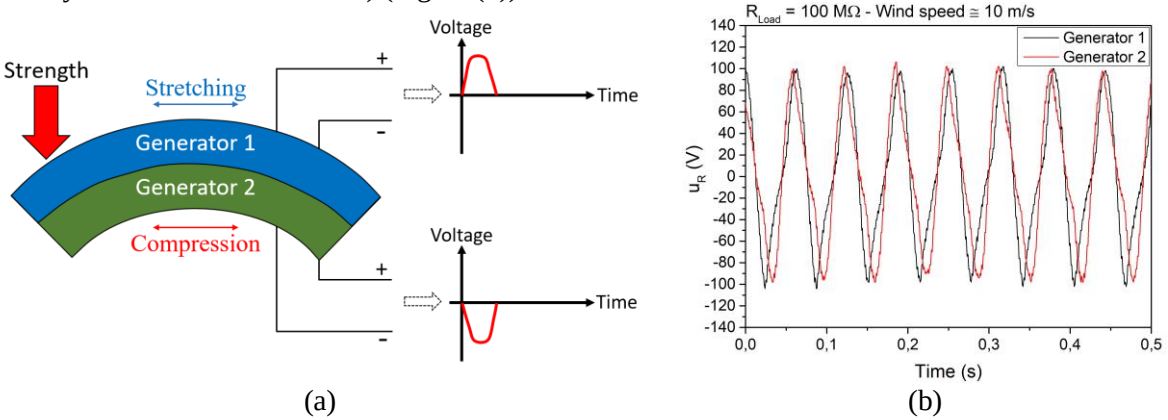

Fig 11 : (a) Representation of the voltages generated during deflection of the bi-generator beam and (b) voltage delivered by the bi-generator beam in galloping configuration for a wind speed of 10 m/s.

The electrical coupling can be designed in two different ways, coupling in series or coupling in parallel of the generators. In the case of our work and taking into account the results obtained previously (high

voltage and low current (Fig 8)), the parallel coupling is the most beneficial. It allows to increase the current generated while keeping a high voltage level.

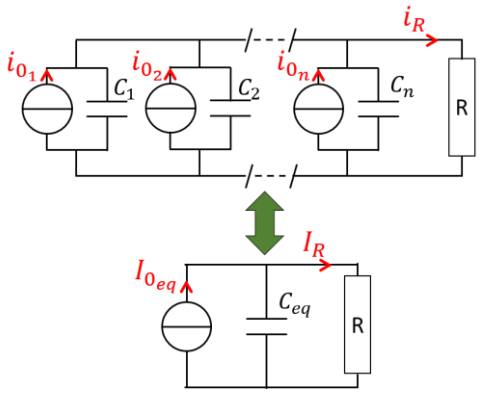

Fig 12 : Equivalent circuit of n micro-generators connected in parallel.

From the equivalent circuit of *n* micro-generators in parallel (Fig 12), we determine the equivalent output current:

$$I_{0_{eq}} = \sum_{x=1}^{n} i_{0_x} \tag{6}$$

The equivalent capacitance of the model is given by:

$$C_{eq} = \sum_{x=1}^{n} C_x \tag{7}$$

The current I_R across the load R is given by:

$$I_R = I_{0_{eq}} \frac{\frac{1}{C_{eq}\omega}}{\sqrt{R^2 + \left(\frac{1}{C_{eq}\,\omega}\right)^2}} = \frac{\sum_{x=1}^{n} i_{0_x}}{\sqrt{R^2\omega^2(\sum_{x=1}^{n} C_x)^2 + 1}} \tag{8}$$

For *n* identical generators, the maximum power ($R = R_{opt} = 1/C\omega$) is given by the formula:

$$P_{max} = \frac{(nI_0)^2}{4\,n\,C\,\omega_{meca}} = \frac{n\,{I_0}^2}{4\,C\,\omega_{meca}} \tag{9}$$

with *n* the number of generators in parallel.

Fig 13 shows the current and voltage amplitudes as a function of the load resistance across the external micro-generator ranging from 1 to 500 MΩ for different wind speeds. The current values gradually decrease to saturation as the load resistance increases. Conversely, the voltage values gradually increase to saturation as the load resistance increases.

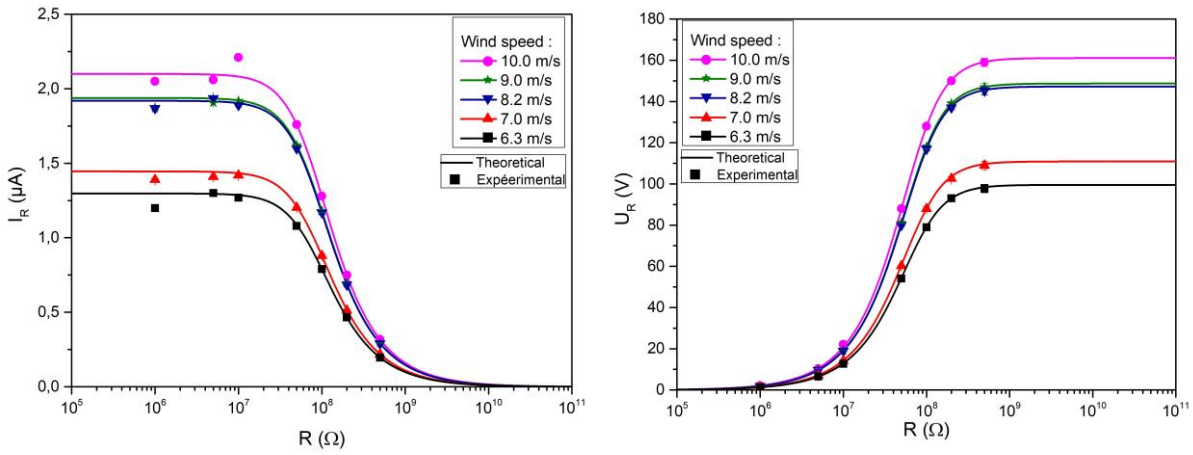

(a) (b)

Fig 13 : (a) Current and (b) voltage amplitudes delivered by the two micro-generators in parallel for different wind speeds as a function of load resistance.

Coupling the two generators in parallel doubled the delivered current from 0.7 µA to 1.3 µA at a wind speed of 6.3 m/s. As for the study with a single generator, the piezoelectric current I_0 also increases significantly with the wind speed. The same trend is also observed for the maximum power, which increases with the wind speed (Fig 14 (a)). It increases from 32 µW for a wind speed of 6.3 m/s to 84 µW with a wind speed of 10 m/s. The evolution of the maximum power delivered by the two-generator configuration as a function of wind speed is plotted in Fig 14 (b).

However, the mechanical coupling of the two generators, had for consequence to increase the total thickness of the beam. This increase in thickness has direct consequences on the wind speeds required to excite the system. The single generator can start to generate energy with a wind speed of 2.3 m/s against 6 m/s for the bi-generator configuration, which can be limiting for the energy harvesting from weak air flow.

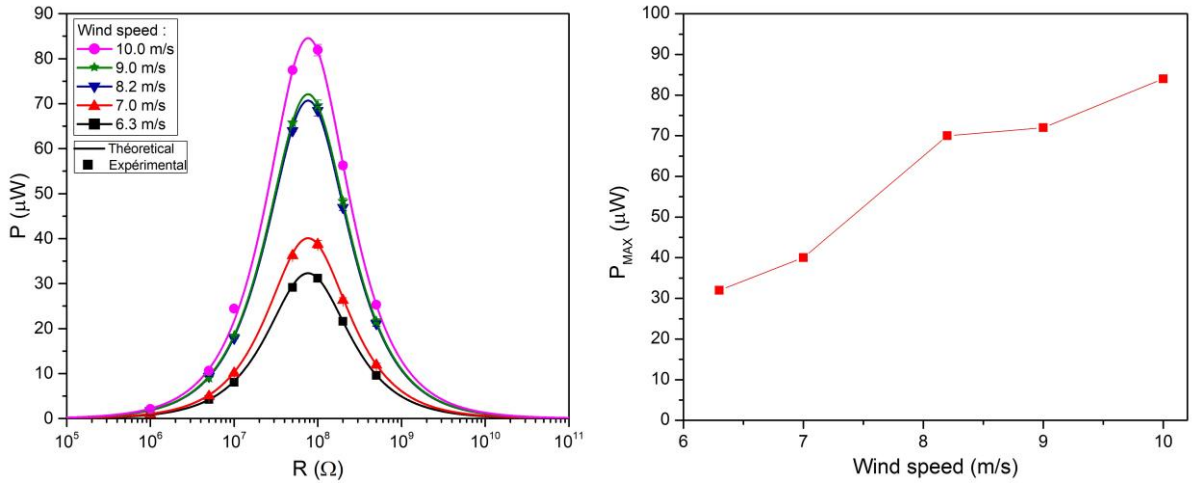

(a) (b)

Fig 14 : (a) Power delivered by the two micro-generators in parallel for different wind speeds as a function of load resistance and (b) evolution of the maximum power delivered by the two micro-generators in parallel as a function of wind speed.

In order to increase the energy harvesting, we have arranged two bi-generator beams on the same fixation and connected them at their ends with the bluff body (Fig 15). The two bi-generator beams being connected together with the bluff body, the four generators will deform simultaneously. Thus, the generators can be directly connected in parallel to increase the current and require only one rectifier circuit.

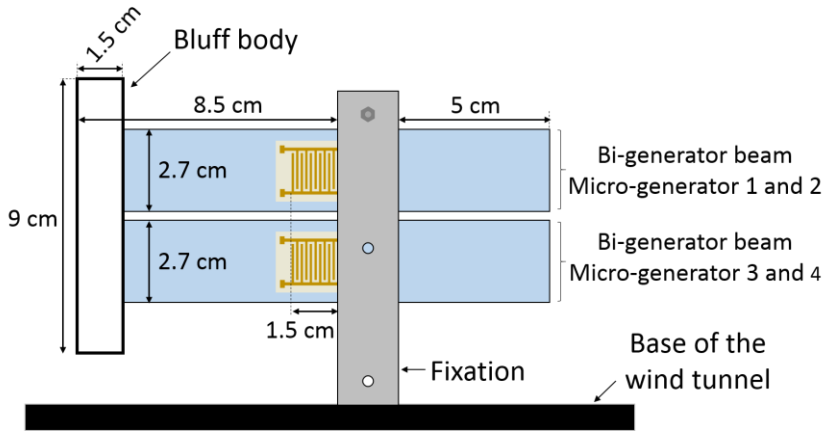

Fig 15 : Schematic of the experimental setup of four generators in in parallel and in galloping configuration.

A comparison between the energy harvesting with one and two bi-generator beams was performed in galloping configuration for a wind speed of 6.3 m/s. The current and voltage amplitudes delivered by the micro-generators are presented in Fig 16 (a) and the power curves in Fig 16 (b). As expected, the coupling of the two bi-generator beams has doubled the maximum power [Eq. (9)] from 30 µW to 60 µW. We can also see that the optimal load resistance has decreased with the paralleling of the four generators. It goes down from 780 kΩ with a bi-generator beam to 410 kΩ with the two bi-generator beams in parallel. This decrease is mainly due to the increase of the total capacitance [Eq. (7)] (from 125 pF to 248 pF for the two bi-generator beams in parallel) but also to the slight increase of the resonance frequency.

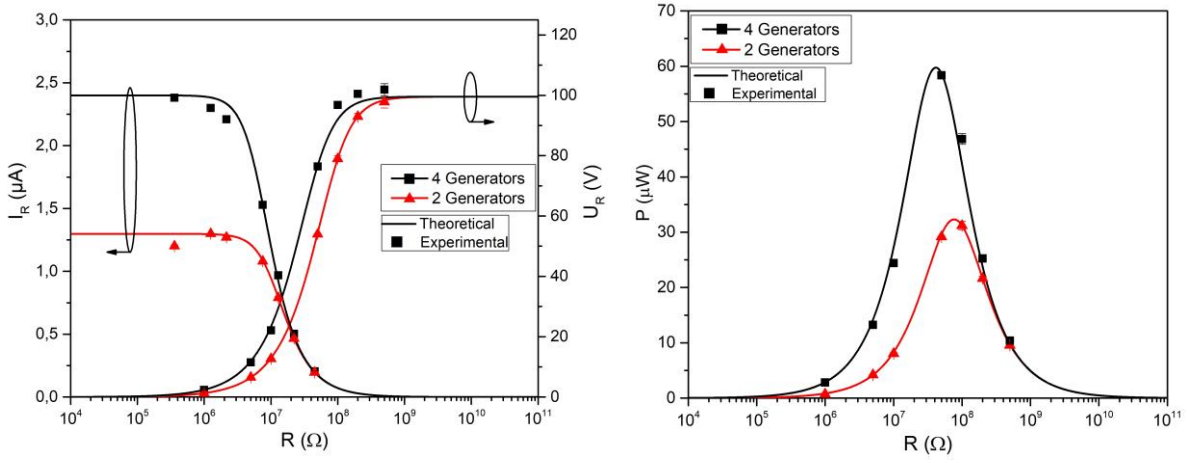

(a) (b)

Fig 16 : Evolution (a) of the voltage and current amplitudes and (b) the power delivered by the four micro-generators in parallel for a wind speed of 6.3 m/s.

To use the micro-generator as a power source for a WSN, the output electrical charge from the generator must be stored in storage elements such as capacitors and batteries. Piezoelectric micro-generators deliver an AC voltage that must be converted to a DC voltage by a rectifier circuit to match the electronic systems to be powered.

3.2 *Power supply of a communicating sensor*

In order to demonstrate the potentialities of the developed coupled generators for self-powering a wireless communicating sensor, we fabricated a complete electronic system consisting of flexible piezoelectric micro-generators, a rectifier bridge (D1N4007 diodes), a storage capacitor (capacitance 1.2 mF), and a commercially available wireless temperature sensor (eZ430-RF2500T, Texas Instruments) as shown in Fig 17. The wireless sensor integrates an ultra-low power microcontroller unit with an internal temperature sensor (MSP430F2274, Texas Instruments), a 2.4 GHz Radio Frequency (RF) transceiver chip (CS2500, Texas Instruments), and a chip antenna, which requires an overall input power greater than 20 mW for 20 ms (corresponding total consumption energy greater than 400 µJ).

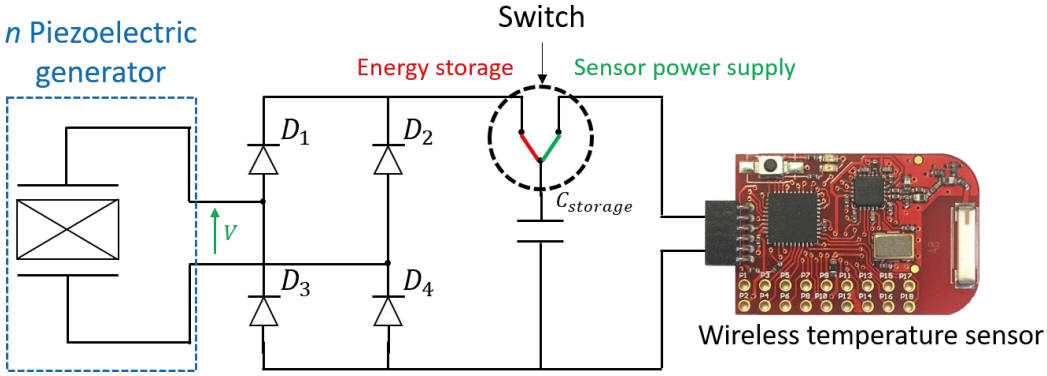

Fig 17 : Electronic schematic for the self-powering of the wireless temperature sensor.

During the periodic cantilever beam bending, an AC voltage is generated by the piezoelectric micro-generators connected in parallel and simultaneously converted, via the rectifier circuit, into DC voltage to charge a 1.2 mF capacitor.

Fig 18 (a) shows the charging curve of the capacitor from 0 to 4.5 V using one or more piezoelectric micro-generators with excitation under constant wind speed (≈ 6.3 m/s). With only one generator, it takes about 5 hours to charge the capacitor to 4.5 V. Although storing energy with the capacitor by flexible micro-generators is generally difficult because of the energy loss due to impedance mismatch, coupling multiple generators in parallel overcomes the energy loss and charges the capacitor. By coupling 4 generators in parallel, the charging time to reach 4.5 V is divided by 5 from 5 hours to 1 hour.
Fig 18 (b) shows the capacitor charge with 4 micro-generators in parallel for different wind speeds. The capacitor charge time decreases with increasing wind speed.

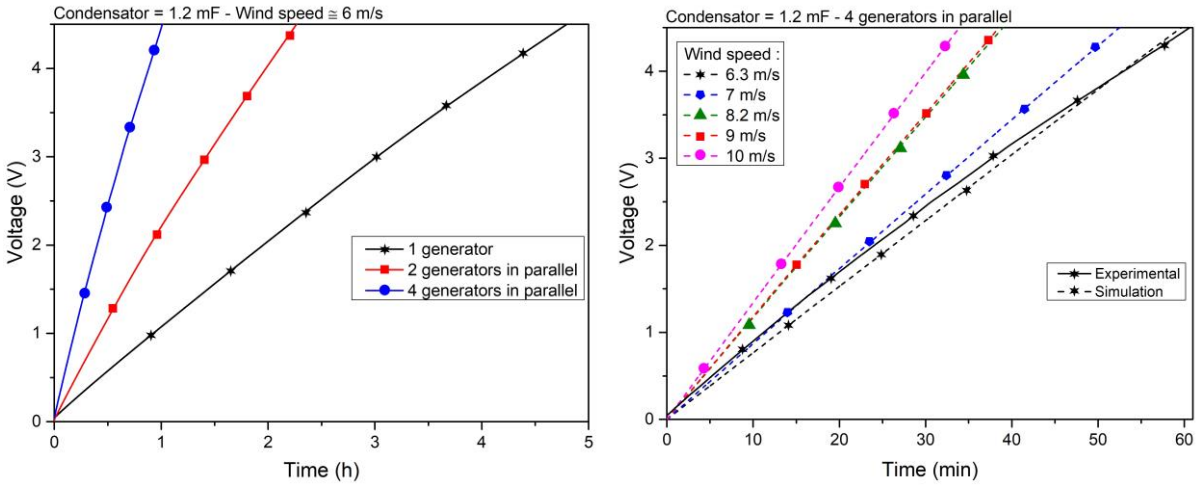

Fig 18 : (a) The charging curve of a capacitor (capacitance 1.2 mF) using 1, 2 and 4 micro-generators in parallel for a wind speed of 6.3 m/s and (b) theoretical and experimental charging curve of capacitor with 4 generators in parallel for different wind speeds.

Finally, the temperature sensor was powered by the charged capacitor to measure the ambient temperature and then wirelessly transmit the information to a 2.4 GHz RF receiver connected to a computer. As shown in Fig 19 (a), the electrical energy from the piezoelectric micro-generators under a wind speed of 6.3 m/s can be used to charge the capacitor from 0 to 4.5 V in about 60 min, and then it is discharged successively to operate the wireless temperature sensor 7 times at intervals of about 4 min. The capacitor voltage immediately dropped to about 3.5 V at about t = 60 min when the sensor was initialized for operation (communication initialization). Another significant voltage drop was observed after the completion of temperature sensing and wireless transmission cycles. The operating time of the sensor can be varied according to the programmed measurement interval to suit the target application (Fig 19 (b)).

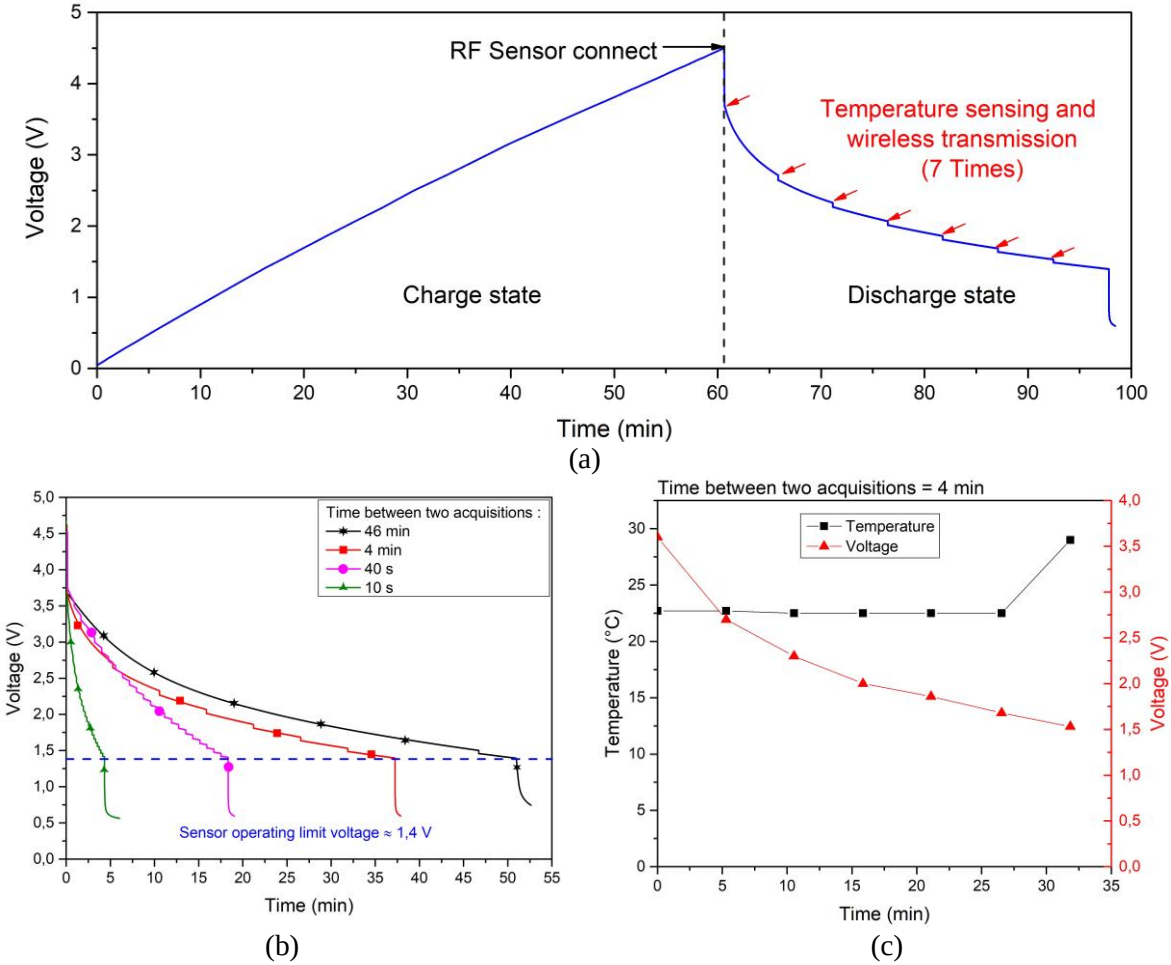

Fig 19 : (a) Charging and discharging curve of a capacitor (capacitance 1.2 mF) for energy storage by the piezoelectric energy harvester and subsequent operation of RF temperature sensor. (b) Discharging curve of the capacitor in the sensor as a function of the time interval between transmissions and (c) Temperature and voltage of the microcontroller recorded and transmitted by the wireless sensor during 32 min.

Fig 19 (c) shows the variation of the ambient temperature in a room at 23.2 °C as well as the supply voltage of the microcontroller as a function of time during 32 min of telecommunication from the RF temperature sensor in order to verify its proper operation.

Finally, this study shows that the flexible aeroelectric energy harvester can be used to make the low-consumption commercial temperature sensor operate in intermittent mode. However, we expect that the operating efficiency of our self-powered WSN system can be significantly improved, in terms of real-time monitoring, by adopting advanced conversion circuits [39–41] or very low power sensor design.

4 Conclusions

In this paper, we have developed and characterized flexible piezoelectric micro-generators for wind energy harvesting. The micro-generator is composed of a thin film of active PZT deposited and annealed on a commercial (low cost) aluminum flexible substrate. The PZT film was then transferred onto a flexible insulate substrate by the chemical process in order to design an IDE structure. Thus, the design steps of the micro-generator are easily transferable to the industry. The flexible PZT micro-generator can convert a maximum output voltage of 100 V and a current signal of 0.7 μA from mechanical bending motions; these values are comparable to those obtained with a flexible piezoelectric all polymer-based energy harvester. Furthermore, our PZT film is advantageous in terms of production cost and processing time to achieve mass production of flexible harvesting devices compared to piezoelectric single crystals that require an expensive and time-consuming process. The novelty of the study lies mainly in the fabrication technique that has been adapted to achieve an ultra-flexible wind micro-generator with high energy efficiency. For an optimal energy harvesting from an air flow, the galloping configuration made it possible to harvest energy from 2.3 m/s wind speed versus 5.5 m/s for the horizontal configurations with and without obstacle. The mechanical and electrical coupling of the micro-generators allowed to increase the maximum recoverable power without increasing the system footprint. To achieve a maximum power output of 60 μW, when the system is excited by a wind of 6.3 m/s in a galloping configuration. Through rectifier elements and a storage capacitor, the energy generated by the system was converted to a DC voltage that could be used by an electronic device. The energy generated by the four generators was used to charge a capacitor to 4.5 V in about 60 minutes to operate a wireless sensor for 35 minutes, allowing the sensor to make 7 measurements and wireless transmission of the ambient temperature. This demonstrate the feasibility of our flexible aeroelectric energy harvesting system for self-powering wireless sensor in the context of Internet of Things (IoT) for specific applications such as structural/environmental monitoring, human health, and military/personal electronics. Thus, their mechanical to electrical energy conversion efficiency, combined with their robustness and flexibility, makes these devices very attractive for aero-electric energy harvesting.

5 Acknowledgements

The authors gratefully acknowledge financial support from the French Region Pays de la Loire via the RFI program WISE.

6 References

[1] J. Wang, S. Zhou, Z. Zhang, D. Yurchenko, High-performance piezoelectric wind energy harvester with Y-shaped attachments, Energy Conversion and Management. 181 (2019) 645–652. https://doi.org/10.1016/j.enconman.2018.12.034.

[2] J. Wang, L. Tang, L. Zhao, Z. Zhang, Efficiency investigation on energy harvesting from airflows in HVAC system based on galloping of isosceles triangle sectioned bluff bodies, Energy. 172 (2019) 1066–1078. https://doi.org/10.1016/j.energy.2019.02.002.

[3] K. Fan, Y. Zhang, S. E, L. Tang, H. Qu, A string-driven rotor for efficient energy harvesting from ultra-low frequency excitations, Appl. Phys. Lett. 115 (2019) 203903. https://doi.org/10.1063/1.5128397.

[4] K. Fan, Y. Zhang, H. Liu, M. Cai, Q. Tan, A nonlinear two-degree-of-freedom electromagnetic energy harvester for ultra-low frequency vibrations and human body motions, Renewable Energy. 138 (2019) 292–302. https://doi.org/10.1016/j.renene.2019.01.105.

[5] Z. Yang, L. Tang, L. Yu, K. Tao, K. Aw, Modelling and analysis of an out-of-plane electret-based vibration energy harvester with AC and DC circuits, Mechanical Systems and Signal Processing. 140 (2020) 106660. https://doi.org/10.1016/j.ymssp.2020.106660.

[6] G. Tang, F. Cheng, X. Hu, B. Huang, B. Xu, Z. Li, X. Yan, D. Yuan, W. Wu, Q. Shi, A Two-Degree-of-Freedom Cantilever-Based Vibration Triboelectric Nanogenerator for Low-Frequency and Broadband Operation, Electronics. 8 (2019) 1526. https://doi.org/10.3390/electronics8121526.

[7] L. Zhang, B. Meng, Y. Xia, Z. Deng, H. Dai, P. Hagedorn, Z. Peng, L. Wang, Galloping triboelectric nanogenerator for energy harvesting under low wind speed, Nano Energy. 70 (2020) 104477. https://doi.org/10.1016/j.nanoen.2020.104477.
[8] K. Fan, Q. Tan, Y. Zhang, S. Liu, M. Cai, Y. Zhu, A monostable piezoelectric energy harvester for broadband low-level excitations, Appl. Phys. Lett. 112 (2018) 123901. https://doi.org/10.1063/1.5022599.
[9] J. Wang, L. Geng, L. Ding, H. Zhu, D. Yurchenko, The state-of-the-art review on energy harvesting from flow-induced vibrations, Applied Energy. 267 (2020) 114902. https://doi.org/10.1016/j.apenergy.2020.114902.
[10] Z. Chen, Y. Xia, J. He, Y. Xiong, G. Wang, Elastic-electro-mechanical modeling and analysis of piezoelectric metamaterial plate with a self-powered synchronized charge extraction circuit for vibration energy harvesting, Mechanical Systems and Signal Processing. 143 (2020) 106824. https://doi.org/10.1016/j.ymssp.2020.106824.
[11] Z. Lu, L.-Q. Chen, M.J. Brennan, T. Yang, H. Ding, Z. Liu, Stochastic resonance in a nonlinear mechanical vibration isolation system, Journal of Sound and Vibration. 370 (2016) 221–229. https://doi.org/10.1016/j.jsv.2016.01.042.
[12] G. Hu, J. Wang, Z. Su, G. Li, H. Peng, K.C.S. Kwok, Performance evaluation of twin piezoelectric wind energy harvesters under mutual interference, Appl. Phys. Lett. 115 (2019) 073901. https://doi.org/10.1063/1.5109457.
[13] D. Huang, S. Zhou, Z. Yang, Resonance Mechanism of Nonlinear Vibrational Multistable Energy Harvesters under Narrow-Band Stochastic Parametric Excitations, Complexity. 2019 (2019) e1050143. https://doi.org/10.1155/2019/1050143.
[14] S.S. Won, H. Seo, M. Kawahara, S. Glinsek, J. Lee, Y. Kim, C.K. Jeong, A.I. Kingon, S.-H. Kim, Flexible vibrational energy harvesting devices using strain-engineered perovskite piezoelectric thin films, Nano Energy. 55 (2019) 182–192. https://doi.org/10.1016/j.nanoen.2018.10.068.
[15] K. Tao, H. Yi, L. Tang, J. Wu, P. Wang, N. Wang, L. Hu, Y. Fu, J. Miao, H. Chang, Piezoelectric ZnO thin films for 2DOF MEMS vibrational energy harvesting, Surface and Coatings Technology. 359 (2019) 289–295. https://doi.org/10.1016/j.surfcoat.2018.11.102.
[16] J. Yang, C. Si, G. Han, M. Zhang, J. Ning, F. Yang, X. Wang, Resonant Properties of a T-sbape Aluminum Nitride Piezoelectric Structure for MEMS Device, in: 2019 International Conference on Manipulation, Automation and Robotics at Small Scales (MARSS), 2019: pp. 1–5. https://doi.org/10.1109/MARSS.2019.8860965.
[17] R. Seveno, D. Averty, Ultra light tunable capacitor based on PZT thin film deposited onto aluminium foil, Journal of Sol-Gel Science and Technology. 68 (2013) 175–179. https://doi.org/10.1007/s10971-013-3149-8.
[18] J. Le Scornec, B. Guiffard, R. Seveno, V. Le Cam, Frequency tunable, flexible and low cost piezoelectric micro-generator for energy harvesting, Sensors and Actuators A: Physical. 312 (2020) 112148. https://doi.org/10.1016/j.sna.2020.112148.
[19] K.-I. Park, J.H. Son, G.-T. Hwang, C.K. Jeong, J. Ryu, M. Koo, I. Choi, S.H. Lee, M. Byun, Z.L. Wang, K.J. Lee, Highly-Efficient, Flexible Piezoelectric PZT Thin Film Nanogenerator on Plastic Substrates, Advanced Materials. 26 (2014) 2514–2520. https://doi.org/10.1002/adma.201305659.
[20] T. Dufay, R. Seveno, B. Guiffard, J.- Thomas, New process for transferring PZT thin film onto polymer substrate, in: 2016 Joint IEEE International Symposium on the Applications of Ferroelectrics, European Conference on Application of Polar Dielectrics, and Piezoelectric Force Microscopy Workshop (ISAF/ECAPD/PFM), 2016: pp. 1–4. https://doi.org/10.1109/ISAF.2016.7578085.
[21] T. Dufay, B. Guiffard, J.-C. Thomas, R. Seveno, Transverse piezoelectric coefficient measurement of flexible lead zirconate titanate thin films, Journal of Applied Physics. 117 (2015) 204101. https://doi.org/10.1063/1.4921588.
[22] R. Seveno, J. Carbajo, T. Dufay, B. Guiffard, J.C. Thomas, Flexible PET/Al/PZT/Al/PET multi-layered composite for low frequency energy harvesting, J. Phys. D: Appl. Phys. 50 (2017) 165502. https://doi.org/10.1088/1361-6463/aa6373.
[23] T. Dufay, B. Guiffard, R. Seveno, S. Ginestar, J.-C. Thomas, Flexible PZT thin film transferred on polymer substrate, Surface and Coatings Technology. 343 (2018) 148–152. https://doi.org/10.1016/j.surfcoat.2017.09.080.

[24] T. Dufay, B. Guiffard, R. Seveno, J.-C. Thomas, Energy Harvesting using a Lead Zirconate Titanate (PZT) Thin Film on a Polymer Substrate, Energy Technology. 6 (2018) 917–921. https://doi.org/10.1002/ente.201700732.
[25] S. Logothetidis, Handbook of Flexible Organic Electronics, 2015. https://books.google.com/books/about/Handbook_of_Flexible_Organic_Electronics.html?hl=fr&id=scjtAwAAQBAJ (accessed September 24, 2019).
[26] J. Zhang, J. Zhang, C. Shu, Z. Fang, Enhanced piezoelectric wind energy harvesting based on a buckled beam, Appl. Phys. Lett. 110 (2017) 183903. https://doi.org/10.1063/1.4982967.
[27] X. He, X. Yang, S. Jiang, Enhancement of wind energy harvesting by interaction between vortex-induced vibration and galloping, Appl. Phys. Lett. 112 (2018) 033901. https://doi.org/10.1063/1.5007121.
[28] W. Sun, F. Guo, J. Seok, Development of a novel vibro-wind galloping energy harvester with high power density incorporated with a nested bluff-body structure, Energy Conversion and Management. 197 (2019) 111880. https://doi.org/10.1016/j.enconman.2019.111880.
[29] X. Yang, X. He, J. Li, S. Jiang, Modeling and verification of piezoelectric wind energy harvesters enhanced by interaction between vortex-induced vibration and galloping, Smart Mater. Struct. 28 (2019) 115027. https://doi.org/10.1088/1361-665X/ab4216.
[30] W. Sun, S. Jo, J. Seok, Development of the optimal bluff body for wind energy harvesting using the synergetic effect of coupled vortex induced vibration and galloping phenomena, International Journal of Mechanical Sciences. 156 (2019) 435–445. https://doi.org/10.1016/j.ijmecsci.2019.04.019.
[31] W. Qin, W. Deng, J. Pan, Z. Zhou, W. Du, P. Zhu, Harvesting wind energy with bi-stable snap-through excited by vortex-induced vibration and galloping, Energy. 189 (2019) 116237. https://doi.org/10.1016/j.energy.2019.116237.
[32] Q. Wang, H.-X. Zou, L.-C. Zhao, M. Li, K.-X. Wei, L.-P. Huang, W.-M. Zhang, A synergetic hybrid mechanism of piezoelectric and triboelectric for galloping wind energy harvesting, Appl. Phys. Lett. 117 (2020) 043902. https://doi.org/10.1063/5.0014484.
[33] J. Wang, C. Zhang, S. Gu, K. Yang, H. Li, Y. Lai, D. Yurchenko, Enhancement of low-speed piezoelectric wind energy harvesting by bluff body shapes: Spindle-like and butterfly-like cross-sections, Aerospace Science and Technology. 103 (2020) 105898. https://doi.org/10.1016/j.ast.2020.105898.
[34] J. Wang, S. Gu, C. Zhang, G. Hu, G. Chen, K. Yang, H. Li, Y. Lai, G. Litak, D. Yurchenko, Hybrid wind energy scavenging by coupling vortex-induced vibrations and galloping, Energy Conversion and Management. 213 (2020) 112835. https://doi.org/10.1016/j.enconman.2020.112835.
[35] J. Zhang, X. Zhang, C. Shu, Z. Fang, Y. Ning, Modeling and nonlinear analysis of stepped beam energy harvesting from galloping vibrations, Journal of Sound and Vibration. 479 (2020) 115354. https://doi.org/10.1016/j.jsv.2020.115354.
[36] M. Shi, A.S. Holmes, E.M. Yeatman, Piezoelectric wind velocity sensor based on the variation of galloping frequency with drag force, Appl. Phys. Lett. 116 (2020) 264101. https://doi.org/10.1063/5.0012244.
[37] J. Zhang, D. Qu, Z. Fang, C. Shu, Optimization of a piezoelectric wind energy harvester with a stepped beam, J Mech Sci Technol. 34 (2020) 4357–4366. https://doi.org/10.1007/s12206-020-1001-y.
[38] G. Hu, J. Wang, L. Tang, A comb-like beam based piezoelectric system for galloping energy harvesting, Mechanical Systems and Signal Processing. 150 (2021) 107301. https://doi.org/10.1016/j.ymssp.2020.107301.
[39] Q. Wei, Energy harvester application of large-deformation-piezoelectrics with synchronized-mechanical-switch circuit, (2017). http://d-scholarship.pitt.edu/31290/ (accessed May 18, 2021).
[40] K. Savarimuthu, R. Sankararajan, S. Murugesan, Analysis and design of power conditioning circuit for piezoelectric vibration energy harvester, IET Science, Measurement & Technology. 11 (2017) 723–730. https://doi.org/10.1049/iet-smt.2016.0377.
[41] A. Brenes, A. Morel, J. Juillard, E. Lefeuvre, A. Badel, Maximum power point of piezoelectric energy harvesters: a review of optimality condition for electrical tuning, Smart Mater. Struct. 29 (2020) 033001. https://doi.org/10.1088/1361-665X/ab6484.